DOI: 10.3901/CJME.2013.02.313, available online at www.springerlink.com; www.cjmenet.com; www.cjmenet.com.cn

Dual Extended Kalman Filter for Combined Estimation of Vehicle State and Road Friction

ZONG Changfu, HU Dan, and ZHENG Hongyu*

State Key Laboratory of Automotive Simulation and Control, Jilin University, Changchun 130022, China

Received February 13, 2012; revised November 18, 2012; accepted December 20, 2012

Abstract: Vehicle state and tire-road adhesion are of great use and importance to vehicle active safety control systems. However, it is always not easy to obtain the information with high accuracy and low expense. Recently, many estimation methods have been put forward to solve such problems, in which Kalman filter becomes one of the most popular techniques. Nevertheless, the use of complicated model always leads to poor real-time estimation while the role of road friction coefficient is often ignored. For the purpose of enhancing the real time performance of the algorithm and pursuing precise estimation of vehicle states, a model-based estimator is proposed to conduct combined estimation of vehicle states and road friction coefficients. The estimator is designed based on a three-DOF vehicle model coupled with the Highway Safety Research Institute(HSRI) tire model; the dual extended Kalman filter (DEKF) technique is employed, which can be regarded as two extended Kalman filters operating and communicating simultaneously. Effectiveness of the estimation is firstly examined by comparing the outputs of the estimator with the responses of the vehicle model in CarSim under three typical road adhesion conditions(high-friction, low-friction, and joint-friction). On this basis, driving simulator experiments are carried out to further investigate the practical application of the estimator. Numerical results from CarSim and driving simulator both demonstrate that the estimator designed is capable of estimating the vehicle states and road friction coefficient with reasonable accuracy. The DEKF-based estimator proposed provides the essential information for the vehicle active control system with low expense and decent precision, and offers the possibility of real car application in future.

Key words: vehicle state, road friction coefficient, estimation, dual extended Kalman filter (DEKF)

1 Introduction

Nowadays, vehicle active safety systems have attracted more attention than ever before due to the dramatically increasing demand for driving safety. Active control systems, such as anti-lock brake system(ABS), traction control system(TCS), and electronic stability program (ESP) have been developed to improve the safety, performance and efficiency of road vehicles. Customarily, the control algorithms involved are designed with the variation of vehicle states(such as the velocity and yaw rate) and driving environment(such as road friction) taken into consideration. For example, the goal of ABS, is to determine a optimal range of road wheel slip ratio that makes the most use of the corresponding tire-road friction, as shown in Fig. 1[1]. However, it is always expensive to measure the vehicle longitudinal velocity for calculating the wheel slip ratio and difficult to detect the road adhension coefficient for determining the optimal slip ratio range.

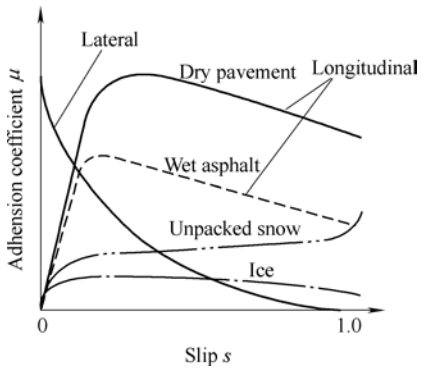

Fig. 1. Adhesion coefficient versus slip curve

In order to reduce the high cost associated with the measurement in active control, many estimation methods have been put forward to acquire vehicle states and road friction coefficient. Kalman filter has become one of the most popular techniques in recent years. Within this research field, BEST, et al[2], completed the combined estimation of vehicle states and parameters by supplementing vehicle parameters (such as the mass m, inertia moment I_z, and the distance between CG and front axle a) into the estimate state vector; but the effect of the change of road friction on state estimation was not considered. RAY, et al[3–4], applied the extended

* Corresponding author. E-mail: zhy_jlu@163.com
This project is supported by National Natural Science Foundation of China(Grant Nos. 51075176, 51105165)

Kalman-Bucy filter to estimate the vehicle states as well as tire forces based on an 8-DOF vehicle model, and compared the estimation results of tire forces with the simulation results from the tire model to determine the road friction coefficient. However, this method calls for hardware with high computational ability due to the complication of the vehicle model. This may cause difficulty in real-time implementation. WENZEL, et al[5–6], accomplished the simultaneous estimation of vehicle states and parameters using dual extended Kalman filter (DEKF) technique based on a 4-DOF vehicle model. This approach utilizes two extended Kalman filter (EKF) working in a parallel with state and parameter estimation and it can be implemented as a single EKF estimator for state or parameter, by simply "turning off" the other estimator. Therefore, it tends to be more flexible than merging them together in one large-scale EKF, as per Best. Nevertheless, no consideration regarding road adhesion has been given. GAO, et al[7] and ZONG, et al[8], respectively put forward the linear and nonlinear estimator based on bicycle model, and compared the estimation results with the off-line vehicle test data. Both works showed good results but suffer to the neglect of the change of road adhesion condition. In conclusion, three essential elements, i.e., the real time performance, the accuracy of estimation and the effect of road friction are ought to be emphasized within the estimation of vehicle dynamics.

In this paper, a DEKF estimator designed based on a three-DOF vehicle model coupled with HSRI tire model is proposed to realize the simultaneous estimation of vehicle states and road friction. Firstly, the 3-DOF vehicle model and HSRI tire model are described in sections 2 and 3, respectively. Then the structure and the detailed design procedure are presented in sections 4 and 5. In section 6, the estimation outcomes are compared with the numerical results from CarSim and driving simulator experiments. Finally in sections 7 and 8, discussions and conclusions are addressed.

2 Vehicle Model

In Fig. 2, the 3-DOF vehicle model to be used for the estimator design is illustrated. This model is capable of representing the essential dynamic properties of a road vehicle, incorporating the longitudinal, lateral and yaw dynamics[9].

The differential equations with respect to the longitudinal, lateral, and yaw dynamics are expressed as Eqs. (1) – (3), respectively:

$$a_x = \dot{v}_x - rv_y, \tag{1}$$

$$a_y = \dot{v}_y + rv_x, \tag{2}$$

$$\dot{r} = \frac{1}{I_z} M_z, \tag{3}$$

where a_x—Longitudinal acceleration of CoG (m/s^2),
a_y—Lateral acceleration of CoG (m/s^2),
v_x—Longitudinal velocity of CoG (m/s),
v_y—Lateral velocity of CoG (m/s),
r—Yaw rate of CoG ((°)/s),
CoG—Centre of gravity,
I_z—Moment of inertia about yaw axis,
I_z=1 353 kg • m^2,
M_z—Torque around the z axle (N • m),

$$M_z = a(F_{x\_\mathrm{fl}}\sin\delta + F_{y\_\mathrm{fl}}\cos\delta + F_{x\_\mathrm{fr}}\sin\delta + F_{y\_\mathrm{fr}}\cos\delta) + \frac{t_\mathrm{f}}{2}(F_{x\_\mathrm{fr}}\cos\delta - F_{y\_\mathrm{fr}}\sin\delta - F_{x\_\mathrm{fl}}\cos\delta + F_{y\_\mathrm{fl}}\sin\delta) - b(F_{y\_\mathrm{rl}} + F_{y\_\mathrm{rr}}) + \frac{t_\mathrm{r}}{2}(F_{x\_\mathrm{rr}} - F_{x\_\mathrm{rl}}), \tag{4}$$

where a—Distance between the CoG and the front axle,
a=1.04 m,
b—Distance between the CoG and the rear axle,
b=1.56 m,
t_f—Front wheel track, t_f=1.481 m,
t_r—Rare wheel track, t_r=1.486 m,
F_x—Longitudinal tire force (N),
F_y—Lateral tire force (N),
fl—Front left wheel,
fr—Front right wheel,
rl—Rear left wheel,
rr—Rear right wheel,
δ—Front wheel angle.

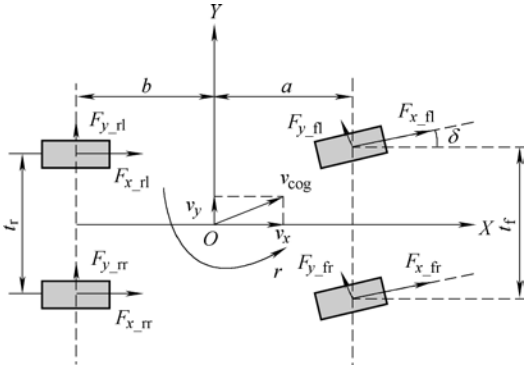

Fig. 2. Three-DOF vehicle model

The longitudinal acceleration a_x and lateral acceleration a_y are determined by Eqs. (5) and (6):

$$a_x = \frac{1}{m}(F_{x\_\mathrm{fl}}\cos\delta - F_{y\_\mathrm{fl}}\sin\delta + F_{x\_\mathrm{fr}}\cos\delta - F_{y\_\mathrm{fr}}\sin\delta + F_{x\_\mathrm{rl}} + F_{x\_\mathrm{rr}}), \tag{5}$$

$$a_y = \frac{1}{m}(F_{x\_\mathrm{fl}}\sin\delta + F_{y\_\mathrm{fl}}\cos\delta + F_{x\_\mathrm{fr}}\sin\delta + F_{y\_\mathrm{fr}}\cos\delta + F_{x\_\mathrm{rl}} + F_{x\_\mathrm{rr}}), \tag{6}$$

where m is the vehicle mass, m=1 231 kg.

3 Tire Model

The choice of tire model would considerably influence the estimation of vehicle states and road friction coefficients in terms of accuracy and real-time property. The widely-used tire models, such as Magic Formula and Unitire, although possess high precision in representing tire dynamics, always involve relatively high computational effort due to the model complexity. This attribute would hinder the accomplishment of real-time estimation. The HSRI tire model, presented by Michigan Highway Safety Research Institute, is a semi-empirical nonlinear tire model[10–11]. Since the structure of this model is relatively simple, as Eqs. (7) and (8), less computational burden is likely to be introduced:

$$F_x=\begin{cases}-c_s\dfrac{s_x}{1-s_x}, & L>1,\\ -c_s\dfrac{s_x}{1-s_x}L(2-L), & L\leqslant 1,\\ -c_s\mu F_z\left[(c_s)^2+(c_\alpha s_y)^2\right]^{-\frac{1}{2}}, & L=0,\end{cases} \tag{7}$$

$$F_y=\begin{cases}-c_\alpha\dfrac{s_y}{1-s_x}, & L>1,\\ -c_\alpha\dfrac{s_y}{1-s_x}L(2-L), & L\leqslant 1,\\ -c_\alpha s_y\mu F_z\left[(c_s)^2+(c_\alpha s_y)^2\right]^{-\frac{1}{2}}, & L=0,\end{cases} \tag{8}$$

where c_s—Tire longitudinal stiffness coefficient,
c_α—Tire cornering stiffness coefficient,
s_x—Longitudinal slip rate of tire,
s_y—Lateral slip rate of tire,
μ—Friction coefficient,
F_z—Vertical tire force (N),

$$L=\frac{1}{2}\mu F_z(1-s_x)\left[(c_s s_x)^2+(c_\alpha s_y)^2\right]^{-\frac{1}{2}}, \tag{9}$$

$$\mu=\mu_0(1-A_s V_s), \tag{10}$$

$$V_s=\sqrt{{s_x}^2+{s_y}^2}\,|V|\cos\alpha, \tag{11}$$

$$V=\sqrt{{V_x}^2+{V_y}^2}, \tag{12}$$

where μ_0—Limiting friction coefficient,
A_s—Vehicle velocity factor,
V—Wheel velocity contacting on ground (m/s)
V_x—Longitudinal component of wheel velocity (m/s),
V_y—Lateral component of wheel velocity (m/s),

Variables involved in the HSRI tire model are expressed as follows:

$$\alpha_{\mathrm{fl,fr}}=\delta-\arctan\left(\frac{v_y+ar}{v_x\mp t_{\mathrm{f}}r/2}\right), \tag{13}$$

$$\alpha_{\mathrm{rl,rr}}=\arctan\left(\frac{-v_y+br}{v_x\mp t_{\mathrm{r}}r/2}\right), \tag{14}$$

$$V_{\mathrm{fl,fr}}=\sqrt{(v_x\mp t_{\mathrm{f}}/2\bullet r)^2+(v_y+a\bullet r)^2}, \tag{15}$$

$$V_{\mathrm{rl,rr}}=\sqrt{(v_x\mp t_{\mathrm{r}}/2\bullet r)^2+(v_y-b\bullet r)^2}, \tag{16}$$

$$s_{x\_ij}=1-\frac{w_{ij}R}{V_{ij}\cos\alpha_{ij}}, \tag{17}$$

$$s_{y\_ij}=\tan\alpha_{ij} \tag{18}$$

$$F_{z\_\mathrm{fl,fr}}=\left(\frac{1}{2}mg\mp ma_y\frac{h}{t_{\mathrm{f}}}\right)\frac{b}{l}-\frac{1}{2}ma_x\frac{h}{l}, \tag{19}$$

$$F_{z\_\mathrm{rl,rr}}=\left(\frac{1}{2}mg\mp ma_y\frac{h}{t_{\mathrm{r}}}\right)\frac{a}{l}+\frac{1}{2}ma_x\frac{h}{l}, \tag{20}$$

$$\delta=\frac{\delta_{\mathrm{w}}}{i_{\mathrm{w}}}, \tag{21}$$

where α—Side-slip angle,
w—Wheel rolling rate (rad/s)
R—Effective rolling radius, R=0.310 8 m,
l—Distance between the front and rare axle,
l=2.6 m,
h—Hight of CoG, h=0.375 m,
δ_{w}—Steering wheel angle,
i_{w}—Ratio of steering wheel angle to front wheel angle.

i_{w} is the steering ratio, i.e. the ratio of steering wheel angle δ_{w} to the front wheel angle δ. It can be found that the variables aforementioned obviously depend on the longitudinal speed v_x, lateral speed v_y, and yaw rate r. The steering wheel angle δ_{w} and wheel speed w_{ij} can be measured using corresponding sensors and have been set up in most of the vehicles that equipped with ABS and ESP. The subscript i denotes the front tire (f) or rear one (r), and j denotes the left tire (l) or right one (r).

The tire stiffness coefficients c_s and c_α are mainly influenced by tire vertical load F_z. In this paper, the tire stiffness coefficients to be used are identified based on the test data of F_x-s and F_y-alpha provided in CarSim. The interpolation method is employed to determine the stiffness values under specific vertical forces, as shown in Table 1.

Table 1. Stiffness coefficient

Vertical tire force F_z/N	1 200	2 400	3 600	4 800
Stiffness coefficient c_s/(N • rad^{-1})	26 500	53 570	84 060	110 230
Stiffness coefficient c_a/(N • rad^{-1})	35 400	70 500	104 000	125 350

4 Structure of DEKF

The DEKF adopts a "boot-strapping" procedure for combined estimation of vehicle state and parameter, using two EKFs operating and communicating in parallel, according to Refs. [12–13], and Refs. [5–6]. The working mechanism of DEKF incorporates the interactive "prediction" and "correction" between two sub-estimators, i.e., the state and parameter estimator, as shown in Fig. 3.

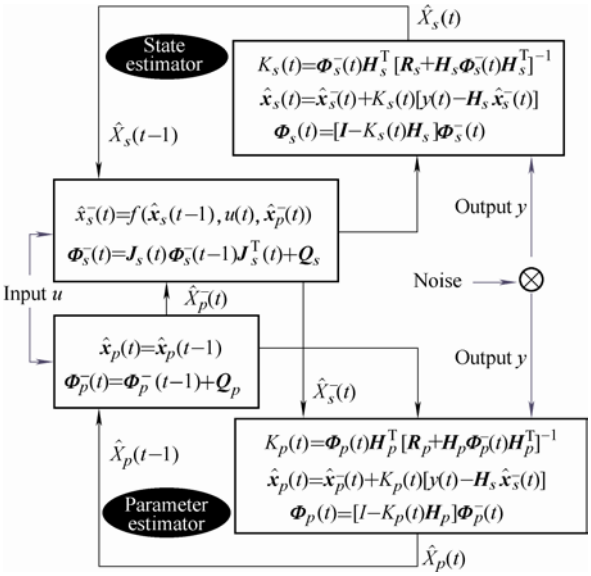

Fig. 3. Dual extended Kalman filter

The state estimator fulfills the tasks of "prediction" and "correction" iteratively. The "prediction" for vehicle state, and error covariance of next time functions as follows:

$$\hat{\boldsymbol{x}}_s^-(t) = f(\hat{\boldsymbol{x}}_s(t-1), u(t), \hat{\boldsymbol{x}}_p^-(t)), \tag{22}$$

$$\boldsymbol{\Phi}_s^-(t) = \boldsymbol{J}_s(t)\boldsymbol{\Phi}_s^-(t-1)\boldsymbol{J}_s^{\mathrm{T}}(t) + \boldsymbol{Q}_s, \tag{23}$$

where the subscript s represents the vectors and matrices associated with vehicle states. $\hat{\boldsymbol{x}}_s^-(t)$ and $\boldsymbol{\Phi}_s^-(t)$ represent the prior estimate for the state and error covariance respectively, and $\boldsymbol{Q}_s$ is the process covariance matrix of the system. $\boldsymbol{J}_s(t)$ can be determined according to Eq. (24):

$$\boldsymbol{J}_s(t) = \exp(\boldsymbol{F}_s(t)\Delta T) = \boldsymbol{I} + \boldsymbol{F}_s(t)\Delta T, \tag{24}$$

where $\boldsymbol{F}_s(t)$ is the Jacobian matrix of $f(\bullet)$ with respect to the state vector $\boldsymbol{x}_s$. ΔT is the sampling time of the system.

The "correction" functionality comprises of three equations respectively for the calculation of Kalman gain, the correction of sate estimation and the correction of error covariance as expressed by Eqs. (25)–(27):

$$K_s(t) = \boldsymbol{\Phi}_s^-(t)\boldsymbol{H}_s^{\mathrm{T}}[\boldsymbol{R}_s + \boldsymbol{H}_s\boldsymbol{\Phi}_s^-(t)\boldsymbol{H}_s^{\mathrm{T}}]^{-1}, \tag{25}$$

$$\hat{\boldsymbol{x}}_s(t) = \hat{\boldsymbol{x}}_s^-(t) + K_s(t)[y(t) - \boldsymbol{H}_s\hat{\boldsymbol{x}}_s^-(t)], \tag{26}$$

$$\boldsymbol{\Phi}_s(t) = [I - K_s(t)\boldsymbol{H}_s]\boldsymbol{\Phi}_s^-, \tag{27}$$

where matrix $\boldsymbol{H}_s(t)$ is the Jacobian matrix of $h(\bullet)$, i.e., the measurement equation, with respect to $\boldsymbol{x}_s$; $\boldsymbol{R}_s$ is the measurement covariance.

The procedure for the design of parameter estimator is similar to that of the state estimator, which also consists of the prediction and correction functionalities, as shown in Eqs. (28)–(32):

$$\hat{\boldsymbol{x}}_p^-(t) = \hat{\boldsymbol{x}}_p(t-1), \tag{28}$$

$$\boldsymbol{\Phi}_p^-(t) = \boldsymbol{\Phi}_p^-(t-1) + \boldsymbol{Q}_p, \tag{29}$$

$$K_p(t) = \boldsymbol{\Phi}_p^-(t)\boldsymbol{H}_p^{\mathrm{T}}[\boldsymbol{R}_p + \boldsymbol{H}_p\boldsymbol{\Phi}_p^-(t)\boldsymbol{H}_p^{\mathrm{T}}]^{-1}, \tag{30}$$

$$\hat{\boldsymbol{x}}_p(t) = \hat{\boldsymbol{x}}_p^-(t) + K_p(t)[y(t) - \boldsymbol{H}_p\hat{\boldsymbol{x}}_p^-(t)], \tag{31}$$

$$\boldsymbol{\Phi}_p(t) = [I - K_p(t)\boldsymbol{H}_p]\boldsymbol{\Phi}_p^-(t), \tag{32}$$

where subscript p represents the vectors and matrices associated with vehicle parameter. $\boldsymbol{H}_p$ is the Jacobian matrix of $h(\bullet)$ with respect to the parameter $\boldsymbol{x}_p$, and $\boldsymbol{R}_p$ is the measurement covariance for the parameter estimator.

5 Algorithm Design of DEKF

Since there is the possibility that the tire-road adhesion condition might change during driving, the friction coefficient can be regarded also as a vehicle parameter, and thus to be estimated using the parameter estimator introduced above. In view of this attribute, the two sub-estimators involved in this paper are designed for vehicle state and road friction estimation, respectively.

5.1 State and measurement equations

Eqs. (1)–(17) are used to define the filter system equation sets $f(\bullet)$ and $h(\bullet)$, as shown in Eqs. (33) and (34):

$$\dot{\boldsymbol{x}}_s(t) = f(\boldsymbol{x}_s(t), \boldsymbol{x}_p(t), u(t), w(t)), \tag{33}$$

$$y(t) = h(\boldsymbol{x}_s(t), \boldsymbol{x}_p(t), v(t)), \tag{34}$$

where the elements in state vector $\boldsymbol{x}_s$ are carefully chosen as

$\boldsymbol{x}_s=(v_x, v_y, r, M_z, a_x, a_y, \alpha_{ij}, s_{x\_ij}, F_{z\_ij})^{\mathrm{T}}$, and the parameter vector is set to be $\boldsymbol{x}_p=(\mu_{\mathrm{fl}}, \mu_{\mathrm{fr}}, \mu_{\mathrm{rl}}, \mu_{\mathrm{rr}})$. Here, α_{ij} indicates $(\alpha_{\mathrm{fl}}, \alpha_{\mathrm{fr}}, \alpha_{\mathrm{rl}}, \alpha_{\mathrm{rr}})$, and s_{x_ij} denotes $(s_{x\_\mathrm{fl}}, s_{x\_\mathrm{fr}}, s_{x\_\mathrm{rl}}, s_{x\_\mathrm{rr}})$. For the convenience of estimator computation, the yaw moment M_z and the vertical forces of four tires F_{z_ij} are included in the state vector. It should be noticed that in this algorithm each tire-road friction is considered as an independent parameter. This feature makes it possible to treat the tire-road friction at different wheels independently when proceeding on an inhomogenous road surface.

The choosing of measurement output for the Kalman filter is greatly depending on the structure of vehicle model and the states to be estimated. In this paper, $y_1(t)=(a_y, r)$ and $y_2(t)=(a_x, a_y)$ are defined as the measurement outputs for the two sub-estimators respectively.

5.2 Calculation of Jacobian matrix

The Jacobian matrices $\boldsymbol{F}_s$, $\boldsymbol{H}_{s1}$ $\boldsymbol{H}_{s2}$ $\boldsymbol{H}_p$ are computated using $f(\bullet)$ and $h(\bullet)$, as shown in Eqs. (35)–(38):

$$\boldsymbol{F}_s=\begin{pmatrix}\dfrac{\partial f_1}{\partial \boldsymbol{x}_{s1}} & \cdots & \dfrac{\partial f_1}{\partial \boldsymbol{x}_{sm}}\\ \vdots & & \vdots\\ \dfrac{\partial f_m}{\partial \boldsymbol{x}_{s1}} & \cdots & \dfrac{\partial f_m}{\partial \boldsymbol{x}_{sm}}\end{pmatrix}=$$

$$\begin{pmatrix}0 & r & v_y & 0 & 1 & 0 & 0 & 0 & 0 & \cdots & 0\\ -r & 0 & -v_x & 0 & 0 & 1 & 0 & 1 & 0 & \cdots & 0\\ 0 & 0 & 0 & 1/I_z & 0 & 0 & 0 & 0 & 0 & \cdots & 0\\ 0 & \vdots & 0 & 0 & 0 & 0 & 0 & 0 & 0 & \cdots & \vdots\\ \vdots & \vdots & 0 & 0 & 0 & 0 & 0 & 0 & 0 & \cdots & \vdots\\ 0 & \vdots & 0 & 0 & 0 & 0 & 0 & 0 & 0 & \cdots & \vdots\end{pmatrix}, \tag{35}$$

$$\boldsymbol{H}_{s1}=\begin{pmatrix}\dfrac{\partial a_y}{\partial \boldsymbol{x}_{s1}} & \cdots & \dfrac{\partial a_y}{\partial \boldsymbol{x}_{sm}}\\ \dfrac{\partial r}{\partial \boldsymbol{x}_{s1}} & \cdots & \dfrac{\partial r}{\partial \boldsymbol{x}_{sm}}\end{pmatrix}=$$

$$\begin{pmatrix}0 & 0 & 0 & 0 & 0 & 1 & 0 & 0 & 0 & \cdots & 0\\ 0 & 0 & 1 & 0 & 0 & 0 & 0 & 0 & 0 & \cdots & 0\end{pmatrix}, \tag{36}$$

$$\boldsymbol{H}_{s2}=\begin{pmatrix}\dfrac{\partial a_x}{\partial \boldsymbol{x}_{s1}} & \cdots & \dfrac{\partial a_x}{\partial \boldsymbol{x}_{sm}}\\ \dfrac{\partial a_y}{\partial \boldsymbol{x}_{s1}} & \cdots & \dfrac{\partial a_y}{\partial \boldsymbol{x}_{sm}}\end{pmatrix}=$$

$$\begin{pmatrix}0 & 0 & 0 & 0 & 1 & 0 & 0 & 0 & 0 & \cdots & 0\\ 0 & 0 & 0 & 0 & 0 & 1 & 0 & 0 & 0 & \cdots & 0\end{pmatrix}, \tag{37}$$

$$\boldsymbol{H}_p=\begin{pmatrix}\dfrac{\partial a_x}{\partial \boldsymbol{x}_{p1}} & \cdots & \dfrac{\partial a_x}{\partial \boldsymbol{x}_{pn}}\\ \dfrac{\partial a_y}{\partial \boldsymbol{x}_{p1}} & \cdots & \dfrac{\partial a_y}{\partial \boldsymbol{x}_{pn}}\end{pmatrix}=\begin{pmatrix}\dfrac{\partial a_x}{\partial \mu_{\mathrm{fl}}} & \cdots & \dfrac{\partial a_x}{\partial \mu_{\mathrm{rr}}}\\ \dfrac{\partial a_y}{\partial \mu_{\mathrm{fl}}} & \cdots & \dfrac{\partial a_y}{\partial \mu_{\mathrm{rr}}}\end{pmatrix}, \tag{38}$$

where $\boldsymbol{H}_{s1}$ represents the Jacobian matrix of $y_1(t)$ with respect to state $\boldsymbol{x}_s$, while $\boldsymbol{H}_{s2}$ is the matrix of $y_2(t)$ with respect to $\boldsymbol{x}_s$. The index m denotes the number of the states to be estimated (m=18) and n the number of parameters (n=4).

In order to make the computation of Jacobian matrix $\boldsymbol{H}_p$ more efficient, the longitudinal slip stiffness c_s and lateral slip stiffness c_α are transformed into:

$$\frac{c_s}{\mu F_z}=c_s^0,\quad \frac{c_\alpha}{\mu F_z}=c_\alpha^0.$$

Therefore, the following expression can be established according to Eq. (9):

$$L=\frac{1}{2}(1-s_x)\left[(c_s^0 s_x)^2+(c_\alpha^0 s_y)^2\right]^{-\frac{1}{2}}.$$

As a result, the relation between the tire force F and road friction μ of the HSRI tire model becomes obvious, as shown below:

$$F_x=\mu F_x^0,\ F_x^0=F_x(F_z, c_s^0, c_\alpha^0, s_x, s_y), \tag{39}$$

$$F_y=\mu F_y^0,\ F_y^0=F_y(F_z, c_s^0, c_\alpha^0, s_x, s_y). \tag{40}$$

5.3 Selection of measurement and process covariances

Usually the measurement covariance $\boldsymbol{R}$ is obtained by taking some off-line sample measurements to represent the sensor noise while the process covariance $\boldsymbol{Q}$ is often used to delineate the uncertainty of the model. Empirically, the performance and convergence of the estimation algorithm are influenced by the selection of the parameters involved in these covariance matrices[14–15]. Therefore, some pre-simulation was conducted to determine a suitable set of measurement and process covariances. Detailedly, it was found the process covariance for the state estimator $\boldsymbol{Q}_s$ need to surpass $10\ 000\,\boldsymbol{I}_{18\times18}$ to guarantee decent estimation. While due to fact that the friction coefficient is no more than 1.2, the selection of covariance $\boldsymbol{Q}_p$ turns out to be much smaller than $\boldsymbol{Q}_s$. The measurement covariances $\boldsymbol{R}_s$, $\boldsymbol{R}_p$ and process covariances $\boldsymbol{Q}_s$, $\boldsymbol{Q}_p$ are finally determined as follows:

$$\boldsymbol{R}_s=\begin{pmatrix}s_{a_x}^2 & 0 & 0\\ 0 & s_{a_y}^2 & 0\\ 0 & 0 & s_r^2\end{pmatrix},\quad \boldsymbol{R}_p=\begin{pmatrix}s_{a_x}^2 & 0\\ 0 & s_{a_y}^2\end{pmatrix}, \tag{41}$$

$$\boldsymbol{Q}_s=10\,000\bullet\boldsymbol{I}_{18\times18},\quad \boldsymbol{Q}_p=0.000\,1\bullet\boldsymbol{I}_{4\times4}, \tag{42}$$

where s_{a_x}, s_{a_y}, s_r represent the noise level of the sensors, which are regarded as 1% range of the measured data of white noise in this paper.

6 Algorithm Simulation and Validation

The designed DEKF algorithm is firstly implemented in Matlab/Simulink in CarSim enviroment. Here the CarSim vehicle model is regarded as a real test vehicle which provides the control inputs and measurement outputs for the DEKF. The numerical values of vehicle states from CarSim are compared with the estimation results delivered by the DEKF algorithm in three typical road adhesion conditions, i.e., the high-friction, low-friction and joint-friction road. The vehicle and tire parameters refer to a B-Class Hatchback which is provided in the above.

6.1 Vehicle states estimation

Before considering the performances of the DEKF algorithm which involves two estimators operating together, the validity of the state estimator is investigated in the first place. For this purpose, the road friction coefficient is set to be known while the parameter estimator for road friction evaluation is temporarily "turned off". Detailedly, a "Double lane change" maneuver at 80 km/h on a road with friction coefficient 0.85 is chosen. The initial values of the EKF algorithm $\hat{\boldsymbol{x}}_0^-$ and $\hat{\boldsymbol{P}}_0^-$ are set as $\hat{\boldsymbol{x}}_0^- = (80/3.6, 0, 0, 0, 0, 0, 0, 0, 0, 0, 0, 0, 0, 0, 0, 1\,000, 1\,000, 1\,000, 1\,000)$, $\hat{\boldsymbol{P}}_0^- = \boldsymbol{I}_{18\times18}$. The estimation results of longitudinal velocity v_x, lateral acceleration a_y and front tire slip angle α_{f} shows good coherences with the outputs fromCarSim(Fig. 4). And the rear left(RL) tire forces calculated by HSRI tire model using the estimated vehicle states also presents excellent consistence with CarSim. These graphical results are believed to be able to confirm the validity of the state estimator in the DEKF structure.

6.2 High friction road estimation

On the basis of section 6.1, both of the state and parameter estimators in the DEKF are "turned on" in this section to perform the combine vehicle state and road friction estimation. An 80° steering wheel step input test with the initial speed of 80 km/h and 50% acceleration pedal is selected. This driving scenario involves both the variation in lateral and longitudinal dynamics and thus believed to be adequately general in representing normal driving conditions. The road friction coefficient in CarSim was set to be 0.8. The input signals of DEKF $u(t) = (\delta, w_{\mathrm{fl}}, w_{\mathrm{fr}}, w_{\mathrm{rl}}, w_{\mathrm{rr}})$ are provided in Fig. 5, and the measurement outputs are set to be $y_1(t) = [a_y, r]$ and $y_2(t) = [a_x, a_y]$.

The initial values of DEKF algorithm $\hat{\boldsymbol{x}}_0^-$ and $\hat{\boldsymbol{P}}_0^-$ are set as $\hat{\boldsymbol{x}}_{s0}^- = (80/3.6, 0, 0, 0, 0, 0, 0, 0, 0, 0, 0, 0, 0, 0, 0, 1\,000, 1\,000, 1\,000, 1\,000)$, $\hat{\boldsymbol{P}}_{s0}^- = \boldsymbol{I}_{18\times18}$, $\hat{\boldsymbol{x}}_{p0}^- = (1, 1, 1, 1)$, $\hat{\boldsymbol{P}}_{p0}^- = 0.02\boldsymbol{I}_{4\times4}$. Fig. 6 shows the estimation values of the tire-road friction coefficients at four wheels. It can be observed that the self-defined initial value set converges to 0.8 quickly. Since the validation of the algorithm on joint friction road (will be presented in section 6.4) will incorporate both state and parameter estimation results on high and low friction road, the comparison between CarSim outputs and the DEKF algorithm is omitted here for brevity, so does that in section 6.3.

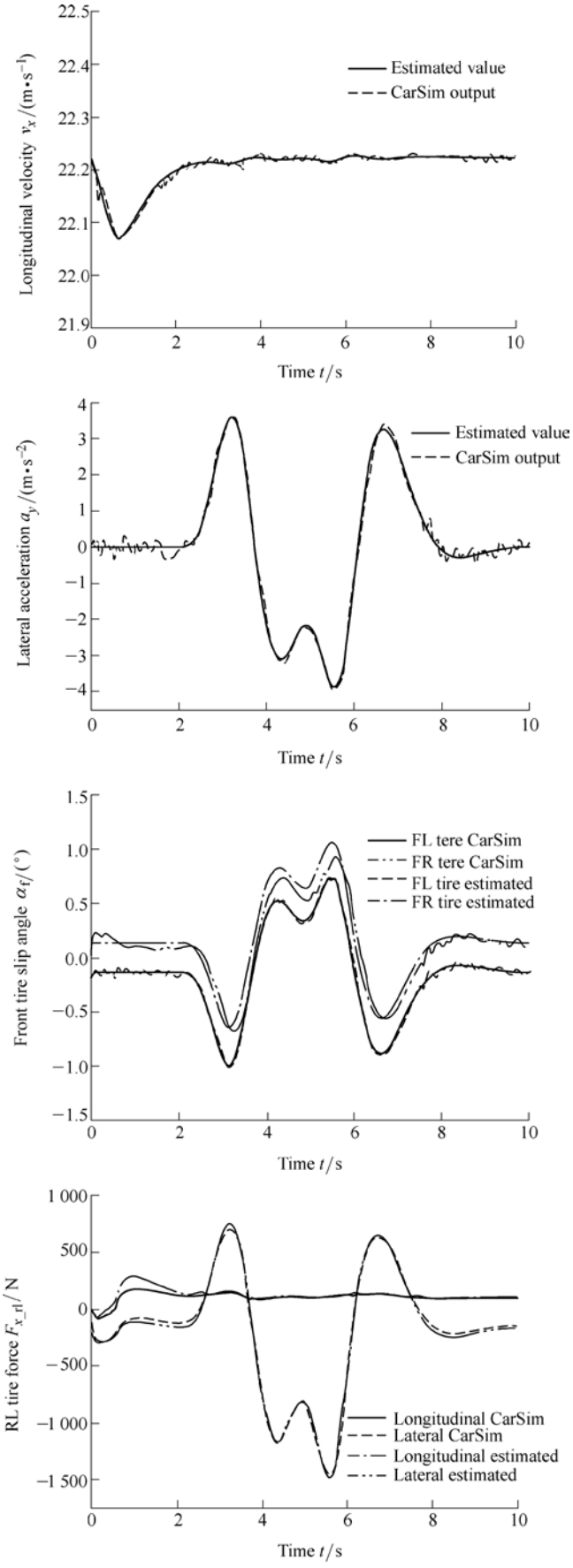

Fig. 4. Vehicle state estimation values

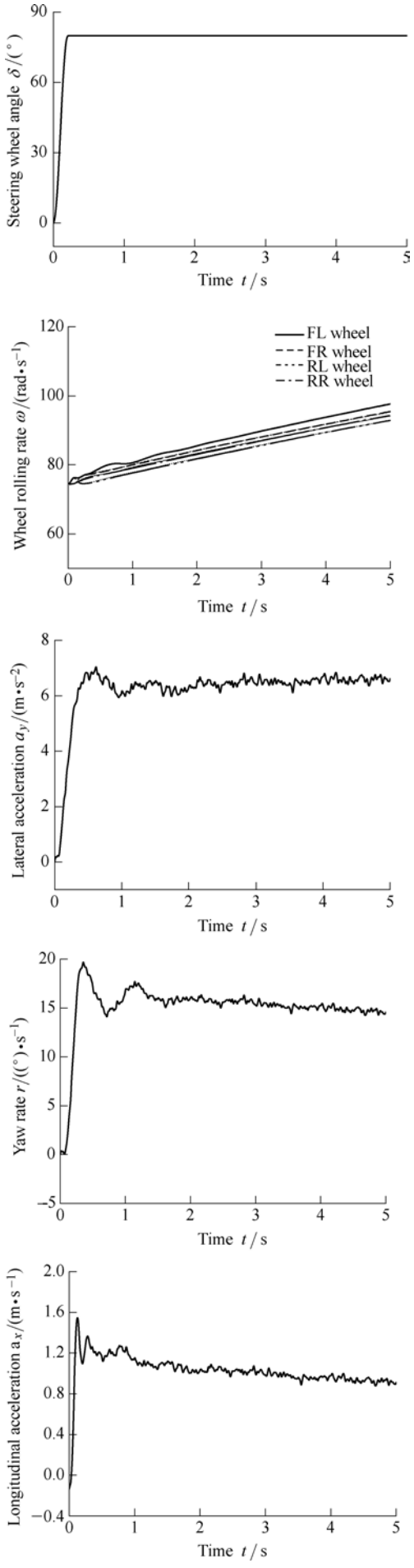

Fig. 5. Input and output of DEKF on high friction road

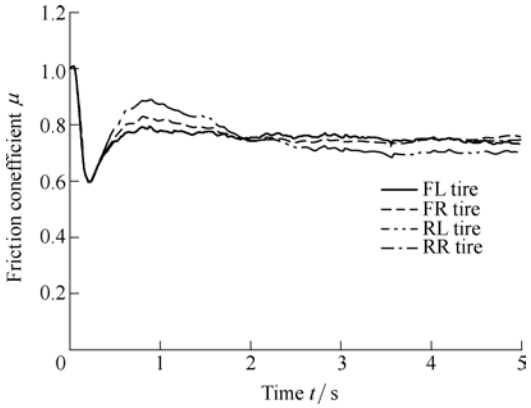

Fig. 6. Estimation values of the tire-road friction coefficients at four wheels

6.3 Low friction road estimation

An 80° steering wheel step input test with the initial speed of 60 km/h is selected while the road friction coefficient is set 0.2 in CarSim. The initial values of $\hat{\boldsymbol{x}}_0^-$ and $\hat{\boldsymbol{P}}_0^-$ are set as $\hat{\boldsymbol{x}}_{s0}^- = (60/3.6, 0, 0, 0, 0, 0, 0, 0, 0, 0, 0, 0, 0, 0, 1\,000, 1\,000, 1\,000, 1\,000)$, $\hat{\boldsymbol{P}}_{s0}^- = \boldsymbol{I}_{18\times18}$, $\hat{\boldsymbol{x}}_{p0}^- = (1, 1, 1, 1)$, $\hat{\boldsymbol{P}}_{p0}^- = 0.02\boldsymbol{I}_{4\times4}$. Fig. 7 illustrates the input and output for the DEKF estimator. The estimation results for the four wheel friction coefficients are presented in Fig. 8. Again, quick convergence from initial value 1 to 0.2 can be captured, which demonstrates the effectiveness of the DEKF algorithm.

6.4 Joint friction road estimation

A steering wheel step input maneuver with the acceleration pedal held at 100% and the initial speed set to be 60 km/h is simulated on a joint adhesion road to deliver a more comprehensive verification towards the DEKF algorithm. Here, the road property is specified as Fig. 9. For a virtual test section with a whole length of 200 m, the adhesion coefficient of the first 40 m section is fixed at 0.8, while the rest at 0.2. Fig. 10 shows the vehicle general trajectory subjecting to this driving scenario. The inconsistency fashion exhibited in the wheel speed time histories is due to the automatic shifting, as shown in Fig. 11. The input and output values for the DEKF are shown in Fig. 12. It also can be observed that the measurement output of the DEKF in "jumps" when the vehicle proceeds from the low friction section to the high one (Fig. 12).

The initial values of $\hat{\boldsymbol{x}}_0^-$ and $\hat{\boldsymbol{P}}_0^-$ are set as $\hat{\boldsymbol{x}}_{s0}^- = (60/3.6, 0, 0, 0, 0, 0, 0, 0, 0, 0, 0, 0, 0, 0, 1\,000, 1\,000, 1\,000, 1\,000)$, $\hat{\boldsymbol{P}}_{s0}^- = \boldsymbol{I}_{18\times18}$, $\hat{\boldsymbol{x}}_{p0}^- = (1, 1, 1, 1)$, $\hat{\boldsymbol{P}}_{p0}^- = 0.02\boldsymbol{I}_{4\times4}$. Fig. 13 shows the estimated values of the vehicle states and four wheel road friction coefficients. To study the impact of the measurement output on estimation results, the parameter estimator applies $y_2(t)^* = [a_y]$ instead of $y_2(t) = [a_x, a_y]$. The road friction estimation results using the measurement output of $y_2(t)^* = [a_y]$ shown in Fig. 14 are not as sound as Fig. 13. This is because that $y_2(t) = [a_x, a_y]$ denotes a mixed

measurement of both longitudinal and lateral movements while $y_2(t)^* = [a_y]$ only represents the lateral dynamics of the vehicle which tends to provide inadequate information for estimating. The deviation of the estimation value of the road friction coefficient from the real value from CarSim is chiefly due to the limitation of the HSRI tire model in terms of capture vehicle dynamics more accurately, but the results is fairly acceptable.

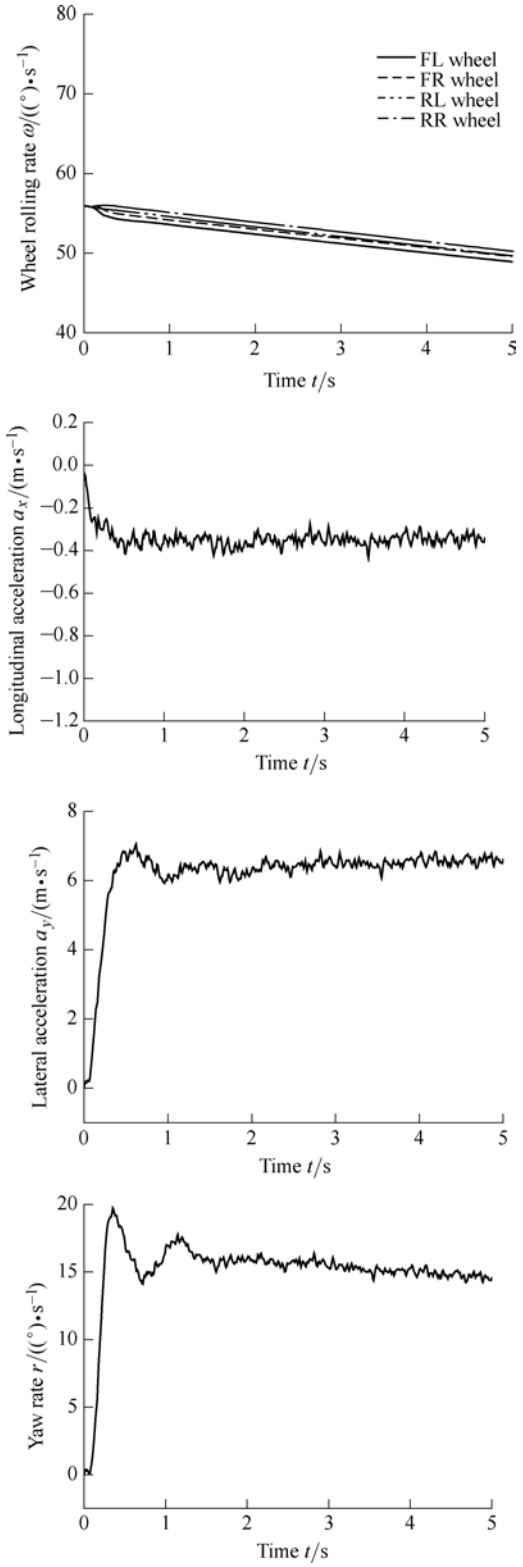

Fig. 7. Input and output of DEKF on low friction road

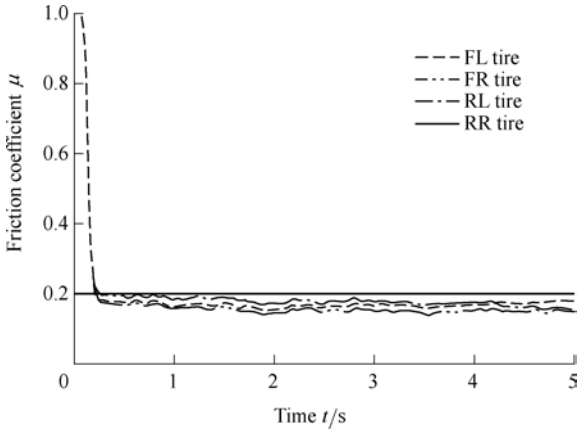

Fig. 8. Road friction coefficient estimation value

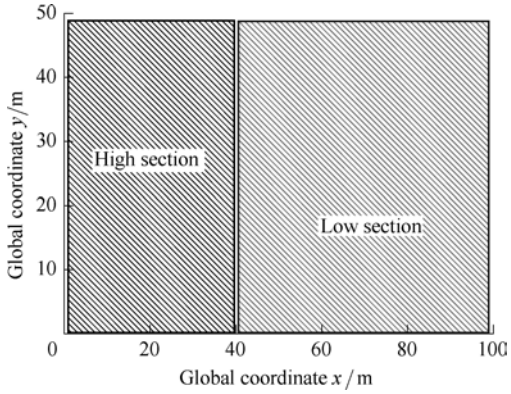

Fig. 9. Road friction coefficient property

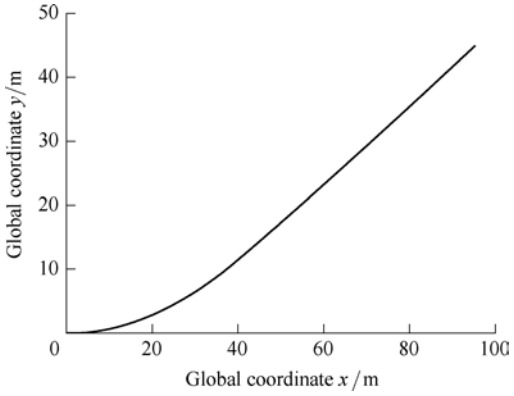

Fig. 10. Vehicle general trajectory

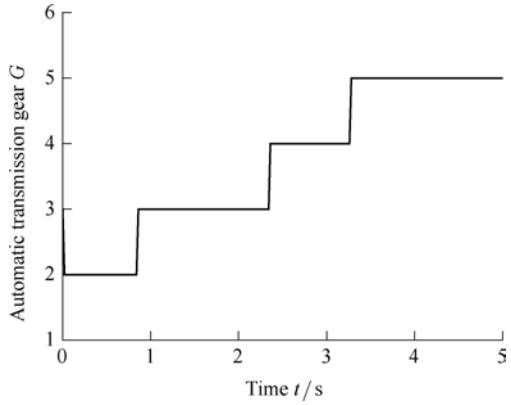

Fig. 11. Shift gears

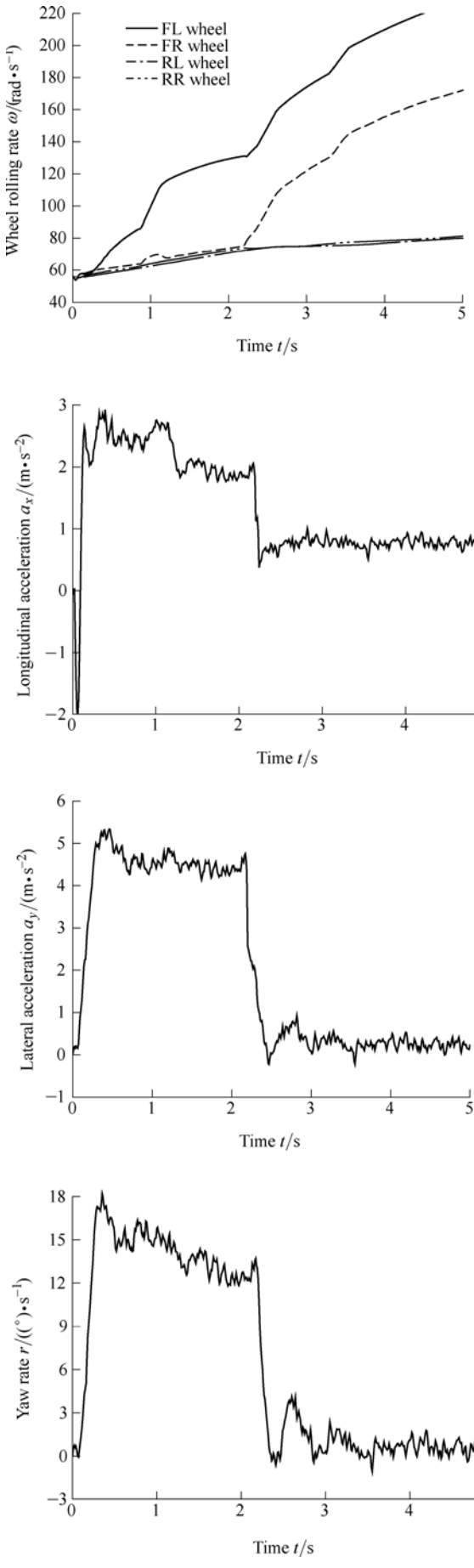

Fig. 12. Input and output of DEKF on joint friction road

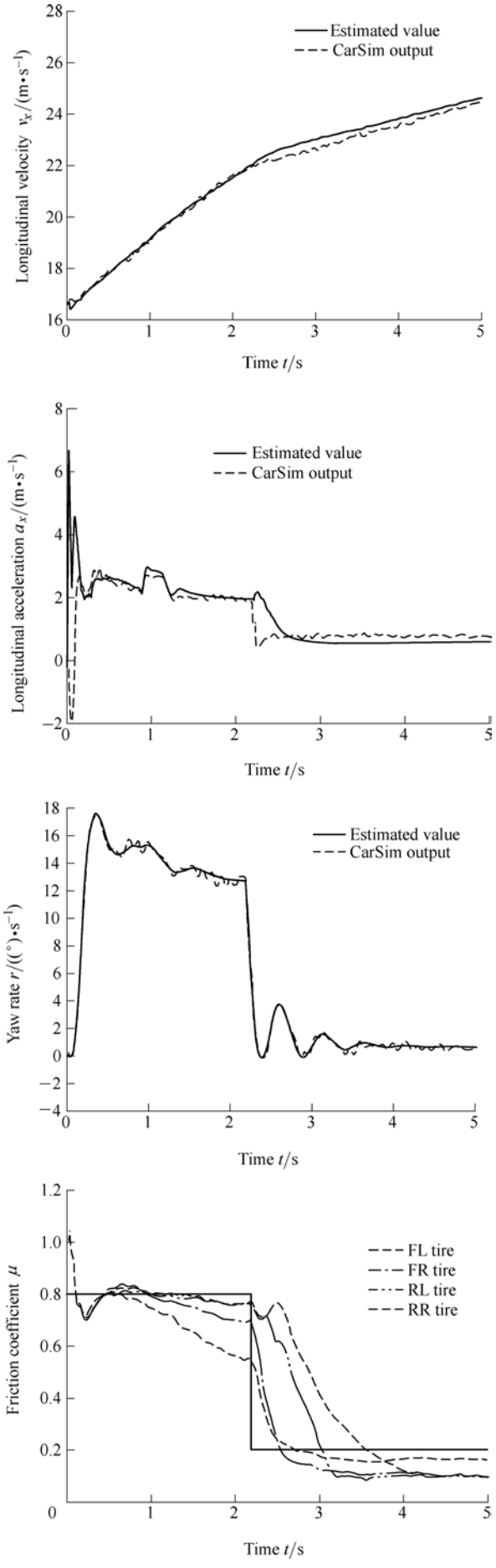

Fig. 13. Estimated values of the vehicle states and four wheel road friction coefficients

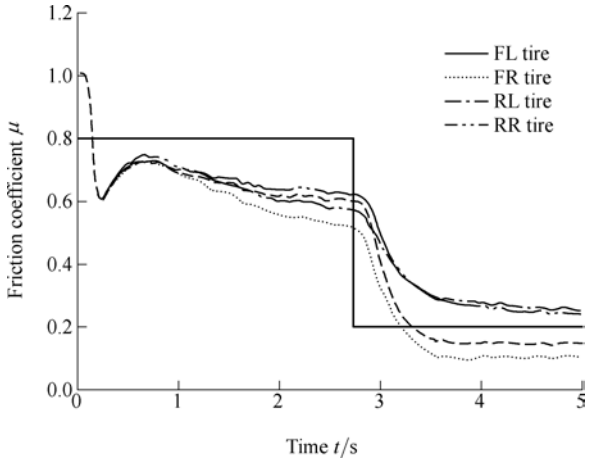

Fig. 14. Road friction coefficient estimation value

The same test was then performed on a more complicated road on which the friction coefficient is set to be 0.8 from 0 to 20 m; 0.2 from 20 m to 40 m; 0.8 from 40 m to 60 m; 0.2 from 60 m to 80 m and 0.8 for the rest. Some of the measurement outputs for the DEKF estimator are provided in Fig. 15. Fig. 16 shows the estimation results of the tire-road friction at front wheels, which trace the change of real road swiftly. Therefore, it can be concluded that the DEKF estimator is also available on friction-quick-change road surfaces.

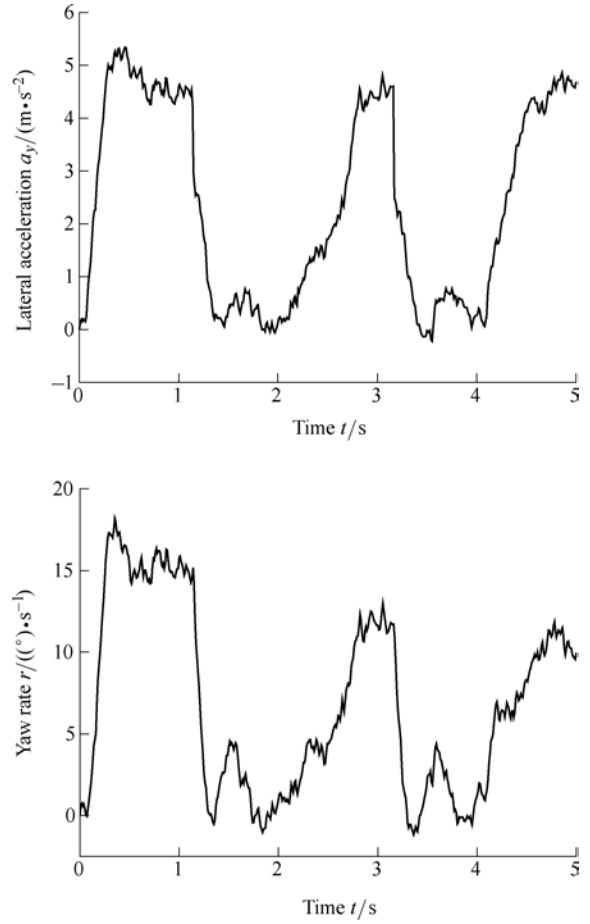

Fig. 15. Measurement output for complicated road surface

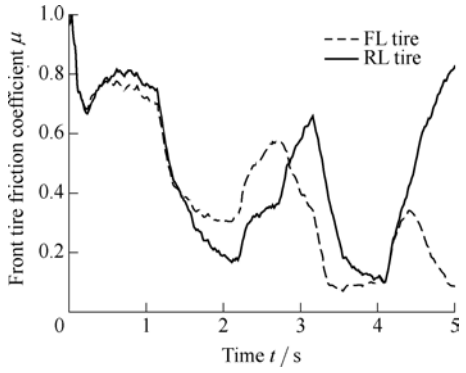

Fig. 16. Estimation results of the tire-road friction at front wheels

6.5 Discussion on significance for considering the change of road friction

It has been reviewed in section 1 that the extended Kalman filter (EKF) was traditionally applied to vehicle states estimation without thorough consideration into the effect of the change road friction coefficient. Assume the real road condition was similar to that shown in Fig. 9, the estimation method of traditional EKF subjecting to constant road friction coefficient would cause grave errors. Corresponding simulation is performed and shown in Fig. 17. It can be seen that the estimated vehicle longitudinal velocity and acceleration based on a constant friction of 0.8 deviate far away from the real values. On the other hand, only small deviation between the estimated longitudinal velocity and the CarSim outputs is found when using DEKF. This state estimation error is mainly caused by the road friction estimation error exhibited in Fig. 13.

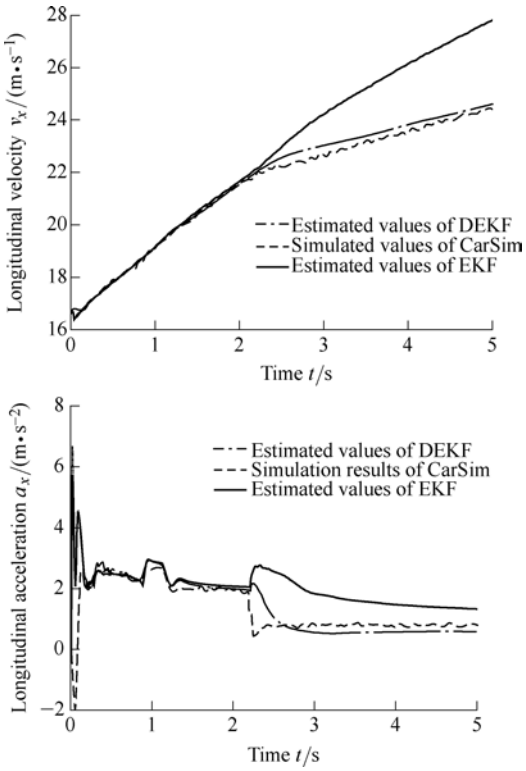

Fig. 17. State estimation comparisons

7 Driving Simulator Experiments

For the purpose of investigating the application of the DEKF in real world situations, the ADSL driving simulator[16] developed by the State Key Laboratory of Automotive Simulation and Control is used to perform simulator experiments. The simulator is assembled partly using real vehicle components such as steering wheel, brake pedal, accelerator pedal, as Fig. 18 shown. The simulator provides a real driving environment for the driver, and meanwhile all the vehicle states and parameters can be exported in real time. Therefore, the validation of the DEKF algorithm on this simulator is believed to be able to represent the potential for its practical application.

Fig. 18. ADSL driving simulator

A braking while curving test on the same joint friction road as Fig. 9 with an initial velocity of 100 km/h was designed and performed on the simulator by the test driver. The travel of steering wheel angle and brake pedal were restricted using some position-limiting block to ensure the repeatability of the experiment. The amplitude of the steering angle input was 60°, and the maximum travel of brake pedal was set to be 10%. Fig. 19 shows the input and output of the DEKF estimator.

The estimated values of the longitudinal velocity, yaw rate and road friction are presented in Fig. 20 which indicate that the DEKF estimator works well with the driving simulator vehicle model. Since there is filtering programs inserted inside the simulator data acquisition system, the signals here are exhibited to be much smoother. The performance of the DEKF estimator currently has not been tested on real vehicles. Nevertheless, due to the real-time dynamics that the driving simulator possesses, the validation of the algorithm on such devices is believed to be able to well predict the application of the estimator on the real vehicles.

8 Conclusions

(1) For the purpose of reducing the computation effort, the estimator is designed based on a 3-DOF dynamic vehicle model coupled with HSRI tire model. The precision of the tire model has been validated.

(2) The key matrices of DEKF are derived from the dynamic equations of vehicle model, and the model parameters are set the same to the vehicle model of CarSim software for simulation validation.

(3) The algorithm is implemented in the Matlab/Simulink environment within the CarSim software. The CarSim provides the input and output variables for the DEKF estimator, and the numerical values for algorithm validating as well.

(4) To interpret the effectiveness of the application of the algorithm on real vehicle, the driving simulator has been used to test the estimation result.

(5) The vehicle state and road friction estimation values show favorable consistency with the data from both of the CarSim and driving simulator, which indicates the effectiveness of the estimation algorithm and the potential for application in real vehicle system.

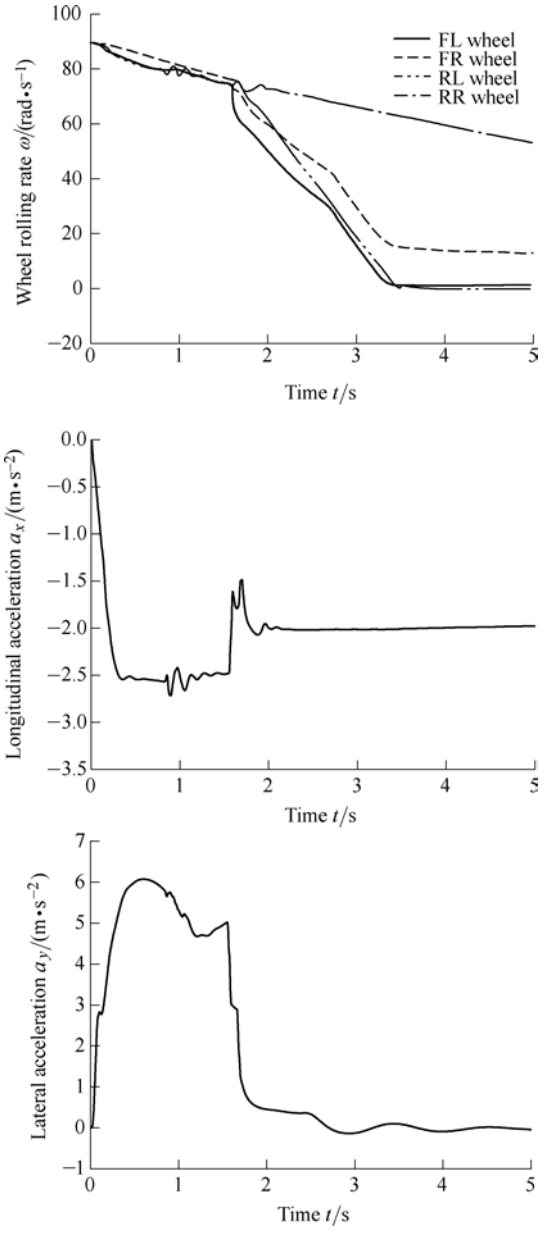

Fig. 19. Input and output of DEKF estimator

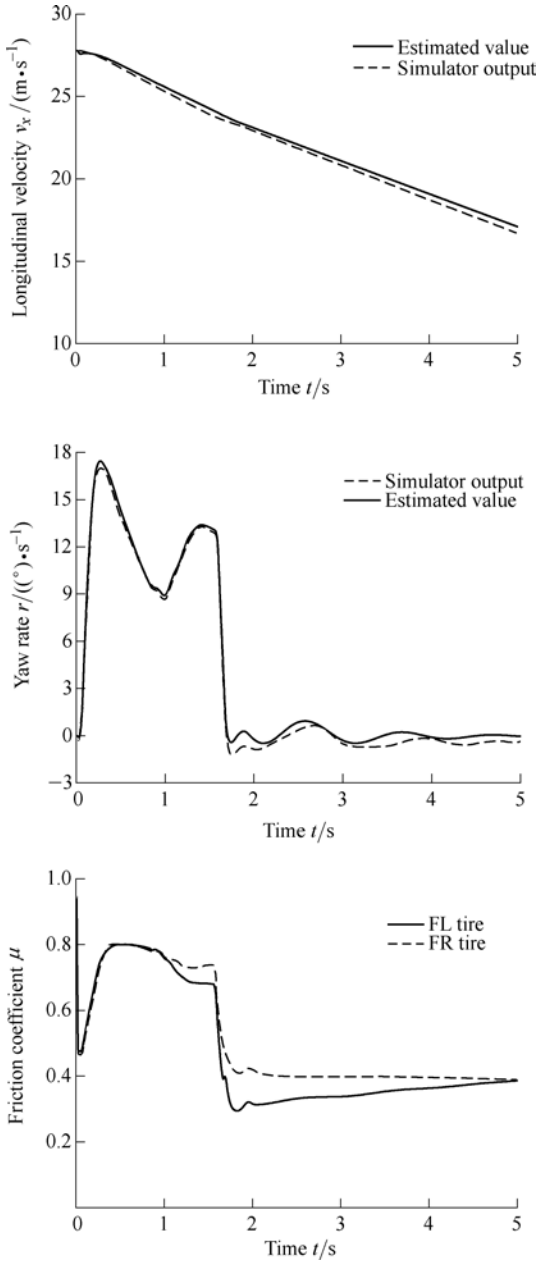

Fig. 20. Estimated values of the longitudinal velocity, yaw rate and road friction

References

[1] WU Mingchin, SHIH Mingchang. Simulated and experimental study of hydraulic anti-lock braking system using sliding-model PWM control[J]. *Mechatronics*, 2003, 13(4): 331–351.

[2] BEST M C, GORDON T J. Combined state and parameter estimation of vehicle handling dynamics[C]//*Proceedings of AVEC 2000 5th Int'1 Symposium on Advanced Vehicle Control*, Ann Arbor, 1Michigan, August, 2000: 429–436.

[3] RAY L R. Nonlinear state and tire force estimation for advanced vehicle control[J]. *IEEE, Transaction on Control Systems Technology*, 1995, 3(1): 117–124.

[4] RAY L R. Experimental determination of tire forces and road friction[C]//*Proceedings of the American Control Conference*, Philadelphia, June, 1998: 1 843–1 847.

[5] WENZEL T A, BURNHAM K J, BLUNDELL M V, et al. Dual extended Kalman filter for vehicle state and parameter estimation[J]. *Vehicle System Dynamics*, 2006, 44(2): 153–171.

[6] WENZEL T A, BURNHAM K J, BLUNDELL M V, et al. Approach to vehicle state and parameter estimation using extended Kalman filtering[C]//*Proceedings of AVEC 2004 7th Int'1 Symposium on Advanced Vehicle Control*, Netherland, August, 2004: 725–730.

[7] GAO Zhenhai, ZHENG Nanning, CHENG Hong. Soft sensor of vehicle state based on vehicle dynamics and Kalman filter[J]. *Journal of System Simulation*, 2004, 16(1): 22–24.

[8] ZONG Changfu, PAN Zhao, HU Dan. Information fusion algorithm for vehicle state estimation based on extended Kalman filter[J]. *Journal of Mechanical Engineering*, 2009, 45(10): 272–277. (in Chinese)

[9] HU Dan, ZONG Changfu. Research on information fusion algorithm for vehicle speed information and road adhesion property estimation[C]//*Proceedings of the 2009 IEEE International Conference on Mechatronics and Automation,* August 9–12, Changchun, China, 2009: 3 229–3 234.

[10] TIELKING J T, MITAL N K. A comparative evaluation of five traction tire models[R]. *Highway Safety Research Institute Report*, Interim Document 6, University of Michigan, January, 1974: 1–27.

[11] DUGOFF H, FANCHER P S, SEGEL L. An analysis of tire traction properties and their influence on vehicle dynamic performance[G]. *SAE Paper,* No. 700377, 1970: 64–66.

[12] WAN E A, NELSON A T. *Kalman filtering and neural networks*[M]. New York: John Wiley & Sons, 2001.

[13] WAN E A, NELSON A T. Neural dual extended Kalman filtering: applications in speech enhancement and monaural blind signal separation[C]//*Proceeding of Neural Networks for Signal Processing Workshop*, IEEE, 1997: 466–475.

[14] KALMAN R E. A vew approach to linear filtering and prediction problems[J]. *Transactions of the ASME — Journal of Basic Engineering*, 1960, 82(D): 35–45.

[15] WELCH G, BISHOP G. *Introduction to Kalman filter*[R]. Department of Computer Science, University of North Carolina at Chapel Hill, NC 27599-3175, 2001.

[16] GUO Konghui, GUAN Hsin, ZONG Changfu. Development an applications of JUT-ADSL driving simulatior[C]// *Proceedings of the IEEE International Conference on Vehicle Electronics,* September 6–9, Changchun, China, 1999: 1–5.

Biographical notes

ZONG Changfu, born in 1962, is currently a professor at *State Key Laboratory of Automotive Simulation and Control, Jilin University, China*. He received his PhD degree from *Jilin University of Technology*, *China,* in 1998. His research interests include automotive simulation and control.
Tel: +86-431-85095090; E-mail: cfzong@yahoo.com.cn

HU Dan, born in 1984, is currently a PhD candidate at *State Key Laboratory of Automotive Simulation and Control, Jilin University, China*.
E-mail: hudan0129@163.com

ZHENG Hongyu, born in 1980, is currently a lecture at *State Key Laboratory of Automotive Simulation and Control, Jilin University, China*. He received his PhD degree from *Jilin University, China*, in 2009. His research interests include automotive simulation and control.
E-mail: zhy_jlu@163.com